Composites Part B 182 (2020) 107624

Contents lists available at ScienceDirect

Composites Part B

journal homepage: www.elsevier.com/locate/compositesb

Mechanically strong and thermally insulating polyimide aerogels by homogeneity reinforcement of electrospun nanofibers

Xingyu Zhao [a], Fan Yang [a], Zicheng Wang [b], Piming Ma [b], Weifu Dong [b], Haoqing Hou [c], Wei Fan [a,**], Tianxi Liu [a,b,*]

[a] State Key Laboratory for Modification of Chemical Fibers and Polymer Materials, College of Materials Science and Engineering, Innovation Center for Textile Science and Technology, Donghua University, Shanghai, 201620, China
[b] Key Laboratory of Synthetic and Biological Colloids, Ministry of Education, School of Chemical and Material Engineering, Jiangnan University, Wuxi, 214122, China
[c] Department of Chemistry and Chemical Engineering, Jiangxi Normal University, Nanchang, 330022, China

ARTICLE INFO

Keywords:
Aerogel
Polyimide
Electrospun nanofiber
Homogeneity
Thermal insulation

ABSTRACT

High-performance thermal insulating materials are greatly needed in many areas. Polyimide aerogels by freeze-drying method have shown great potential as thermal insulating materials. Improving the mechanical performance of polyimide aerogels, meanwhile without deteriorating their thermal insulating performance, is very significative. In this work, a significant homogeneity reinforcement of polyimide aerogels has been achieved by using electrospun polyimide nanofibers as the reinforcing fillers. Short nanofibers could improve strength and toughness of polyimide aerogels by dispersing stress along the pore wall and nanofibers via mechanical interlocking effect due to the good compatibility between them. Consequently, the nanofiber-reinforced polyimide (NRPI) aerogels exhibit better structural formability and excellent mechanical performance, showing compressive modulus of 3.7 MPa with a density of 54.4 mg cm^{-3}, nearly twice that of neat polyimide aerogel. More importantly, owing to the high porosity and intertwined three-dimensional network, NRPI aerogels exhibit better thermal insulating properties compared with commercial insulating materials, especially at high temperatures. Therefore, the nanofiber reinforced polyimide aerogels with good mechanical performance are promising candidates for thermal insulating applications.

1. Introduction

Nowadays, the total energy consumption worldwide is still growing and it is essential to reduce the energy consumption [1–4]. Heat energy management is of great importance since energy loss is mainly dissipated in the form of heat energy [5]. Except exploring new resources, developing thermal insulating materials and reducing heat transfer is one of the most useful ways to reduce energy loss and improve energy efficiency [4,6–9]. Commercial thermal insulating materials including mineral wool, fiberglass, polyurethane (PU), expanded polystyrene (PS), and so on, exhibit thermal conductivity in the range of 30–80 mW m^{-1} K^{-1}. However, these thermal insulating materials either suffer from inferior mechanical properties or poor thermal stability. Moreover, further reducing the thermal conductivity is highly desirable for thermal insulation applications in extreme conditions [10].

Since the 20th century, aerogels, which own low density and high thermal insulating performance, are widely used in thermal insulating areas [11,12]. Aerogel is defined as a gel that consists of a microporous solid with gas as the dispersed phase [13]. As a typical inorganic aerogel, SiO_2 aerogel owns low thermal conductivity, which can be used in high temperature environment [14,15]. However, owing to their brittle nature and crystallization-induced pulverization behaviours, SiO_2 aerogels exhibit high modulus but low toughness [16]. Therefore, they would suffer from serious strength degradation and structural collapse under external force.

Compared with inorganic aerogels, polymer aerogels own both good thermal insulating and mechanical performance [17–20]. Among the polymer aerogels, polyimide aerogels exhibiting excellent mechanical properties and high-temperature stability have drawn much attention recently [21–23]. Normally, polyimide aerogels can be fabricated via

* Corresponding author. State Key Laboratory for Modification of Chemical Fibers and Polymer Materials, College of Materials Science and Engineering, Innovation Center for Textile Science and Technology, Donghua University, Shanghai, 201620, China.
** Corresponding author.
E-mail addresses: weifan@dhu.edu.cn (W. Fan), txliu@dhu.edu.cn, txliu@fudan.edu.cn (T. Liu).

https://doi.org/10.1016/j.compositesb.2019.107624
Received 24 September 2019; Received in revised form 23 November 2019; Accepted 25 November 2019
Available online 28 November 2019

sol-gel transition, supercritical carbon dioxide drying or freeze-drying, followed by chemical or thermal imidization. Compared with supercritical drying, freeze-drying method has several advantages, such as green, simple and inexpensive. However, polyimide aerogels prepared by freeze-drying method normally exhibit inferior mechanical performance due to the large ice crystals formed during the freezing process [24]. Therefore, improving the strength of polyimide aerogels by freeze-drying method, meanwhile without deteriorating its thermal insulating performance, is very significative.

Introducing reinforcing fillers into the polymer matrix is an efficient way to improve the mechanical performance of composite materials [25]. Nanofillers such as SiO_2 nanoparticles [17], carbon nanotubes [18], MXene [26] graphene [27], boron nitride [28] and clay [29] have been used to fabricate polyimide composite aerogels. For example, lightweight and superelastic MXene/polyimide aerogels have been reported by freeze-drying, showing a compressive stress of 0.17 MPa at 50% strain [26]. Reduced graphene oxide/polyimide aerogel prepared by freeze-drying shows a compressive stress of 2.5 kPa at 50% strain [27]. A polyimide/clay aerogel has been reported by Wu et al. by freeze-drying, which show compressive modulus of 0.33 MPa with a density of 90 mg cm^{-3} [29]. These nanofillers reinforced polyimide aerogels still exhibit limited mechanical performance, which is probably due to the poor dispersion of nanofillers in polymer matrices as well as weak interfacial adhesion between the filler and matrix originated from the heterogeneity or incompatibility of fillers and matrix. Therefore, homogeneity reinforcement of polyimide aerogels provides a promising solution for the mechanical improvement of composite materials.

In this work, we report a significant homogeneity reinforcement of polyimide aerogels using short electrospun polyimide nanofibers as reinforcing phase. It is found that the short nanofibers could help stress transfer via mechanical interlocking effect within polyimide matrix, thus avoiding stress concentration and supporting the whole framework of composite materials. The nanofiber-reinforced polyimide (NRPI) aerogels exhibit improved structural formability and mechanical performance, showing compressive modulus of 3.7 MPa with a low density of 54.4 mg cm^{-3}. Moreover, owing to the high porosity and intertwined three-dimensional (3D) network, NRPI aerogels exhibit better thermal insulating properties compared with commercial insulating materials, especially at high temperatures. Therefore, the NRPI aerogels with both high strength and toughness may find wide application prospects in the fields of building, aerospace and high temperature reaction catalyst carriers.

2. Experiment

2.1. Fabrication of short polyimide nanofibers

The short polyimide nanofibers were prepared by electrospinning, thermal imidization followed by cutting. First, 4,4′-oxidianiline (ODA) (0.01 mol) was completely dissolved in 50 mL N,*N*-dimethylacetamide (DMAc). Then, 3,3′,4,4′-biphenyltetracarboxylic dianhydride (BPDA) (0.012 mol) was slowly added into the above solution with intense stirring at 0 °C for 10 h. The resultant poly(amic acid) (PAA) solution was diluted to 4 wt% by DMAc and applied for electrospinning process. The applied voltage is 20 kV, and the bolus speed is 0.055 mm min^{-1}. The aligned nanofibers were collected by a rotating disk (width: 3 cm, diameter: 15 cm) with a speed of 1500 rpm. The as-prepared PAA nanofiber membranes were first dried in vacuum at 70 °C for 6 h and then thermally imidized to obtain aligned polyimide nanofiber membranes. The imidization process is carried out in nitrogen atmosphere with a tube furnace by heating to 150 °C and kept for 30 min followed by heating to 350 °C and kept for 60 min. Finally, the obtained polyimide nanofibers were cut into short polyimide nanofibers with different lengths (processed by Jiangxi Advanced Nanofiber S&T Co., Ltd.).

2.2. Fabrication of nanofiber-reinforced polyimide (NRPI) aerogels

Triethylamine (TEA) capped PAA oligomer was fabricated according to our previous work [17]. 3 g of TEA capped PAA and 2 g TEA were completely dissolved in deionized water. Afterwards, 0.3 g short polyimide nanofibers were added into the PAA solution and homogenized by the homogenizer (IKA T25, Germany) for 30 min, forming uniform dispersions. Afterwards, the dispersions were poured into a desired mould, frozen in liquid nitrogen, then freeze-dried for 72 h with a freeze-dryer (FreeZone, Labconco Corporation, USA) to obtain the pre-NRPI aerogel. Finally, the obtained precursor aerogel was heated to 150 °C and kept for 30 min followed by heating to 350 °C and kept for 60 min for imidization of PAA into polyimide. The obtained nanofiber-reinforced polyimide (NRPI) aerogels were indexed as NRPI-x, in which x represents the content of short polyimide nanofibers. Besides, NRPI aerogels by adding short polyimide nanofibers with different lengths were also fabricated for comparison.

3. Result and discussion

The preparation of nanofiber-reinforced polyimide (NRPI) aerogels is schematically described in Fig. 1A. Specifically, short polyimide nanofiber was obtained by electrospinning, thermal treatment and homogenization. The polyimide nanofibers (length about 300 μm, diameter about 400 nm, Fig. S1) were mixed with water soluble poly(amic acid) (PAA) to form a homogeneous suspension, in which short polyimide nanofibers can be dispersed uniformly (photograph shown in step 2). Moreover, the resulting homogeneous dispersion could remain stable without any sedimentation. After the following freeze-drying and thermal imidization, NRPI aerogels can be obtained (photograph shown in step 3). The samples are indexed as NRPI-x, in which x represents the content of short polyimide nanofibers. The aerogels show good structural formability and can be tailored into different shapes, such as triangular, prism and cylinder. Moreover, NRPI aerogels could be shaped into a cuboid on large scale (Fig. 1B). The resulting NRPI aerogel could withstand 700 g weight (about 2000 times of NRPI aerogel) with no deformation, indicating its excellent anti-compressibility (Fig. 1C). Meanwhile, the NRPI aerogels exhibit a low density of 54.4 mg cm^{-3} and could freely stand on stamen (Fig. 1D), indicating its lightweight nature.

Scanning electron microscope (SEM) images of NRPI aerogels with or without short polyimide nanofibers are shown in Fig. 2. As shown in Fig. 2A and B, polyimide aerogels without adding short polyimide nanofibers, exhibit uniform 3D porous structure with smooth lamellar pore walls and pore size of ~50 μm. With 10% short polyimide nanofibers as reinforcement, NRPI-10 remains the 3D porous structure and exhibits a cellular honeycomb-network with nanofibers interconnected with lamellae (Fig. 2C). SEM images indicate that the short polyimide nanofibers are closely attached with polyimide lamellae and arranged to form oriented filament architecture (Fig. 2D). Besides, the short polyimide nanofibers are homogeneously distributed in polyimide aerogels, which can be attributed to the good interfacial interaction between the matrix and the short nanofibers. By varying the nanofiber content, the NRPI aerogels exhibit similar cellular honeycomb-network as for NRPI-5 and NRPI-20 (Fig. S2). With the content of short polyimide nanofibers increased, more short polyimide nanofibers could be obviously observed from SEM images.

As is well known, polyimide aerogels produced by freeze-drying and thermal treatment would suffer from severe volume shrinkage, because of the thermal stress shock during thermal imidization process. On the contrary, by adding short polyimide nanofibers into the polyimide matrix, shrinkage of the aerogels is inhibited obviously (Fig. 3A). With the increase of nanofiber content, the shrinkage rate of NRPI aerogels is decreased from 42% to 20% with short polyimide nanofiber content of 20%, exhibiting much better structural formability (Fig. 3B). This can be attributed to the fact that short polyimide nanofibers could share the thermal stress and support aerogel structure during thermal imidization

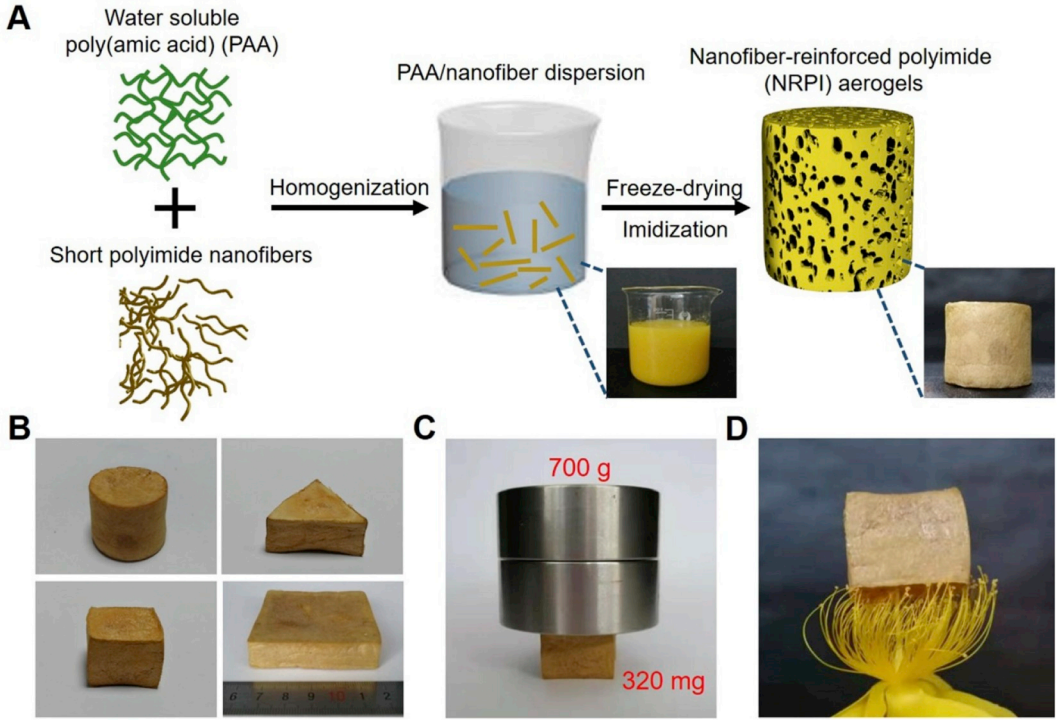

Fig. 1. Structure design and architecture of nanofiber-reinforced polyimide (NRPI) aerogels. (A) Schematic illustration of preparation of NRPI aerogels. (B) Photograph of NRPI aerogels with different shapes. (C) Photograph of NRPI aerogel that could withstand over 2000 times of its own weight. (D) Photograph showing NRPI aerogel standing on stamen.

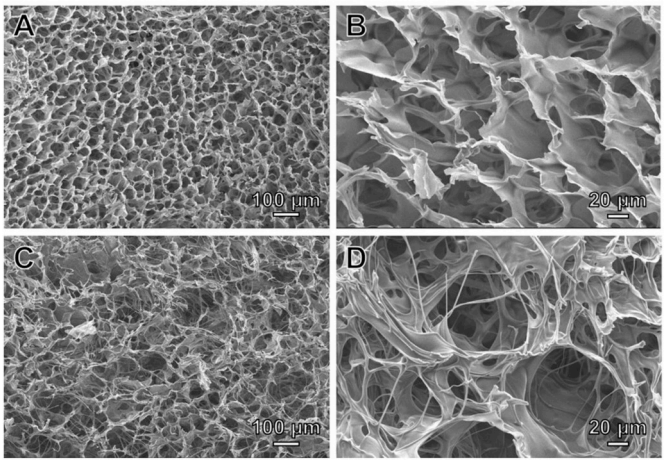

Fig. 2. Morphology of NRPI aerogels. (A and B) SEM images of NRPI-0 aerogel with different magnifications. (C and D) SEM images of NRPI-10 aerogel with different magnifications.

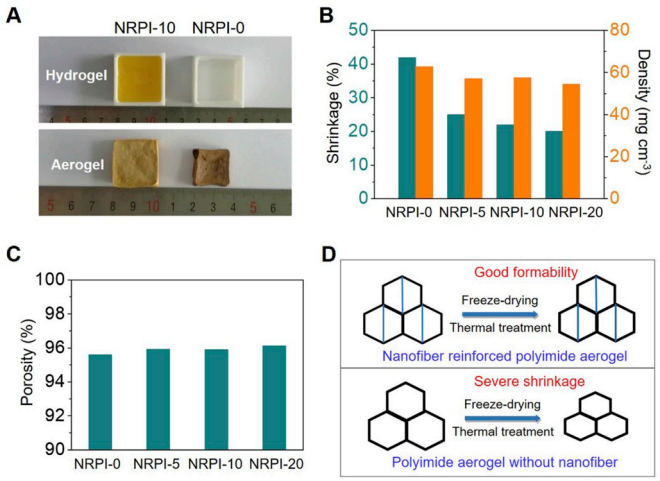

Fig. 3. Structural formability and dimensional stability of NRPI aerogels. (A) Photograph of NRPI-0 and NRPI-10 before and after freeze-drying and thermal treatment, indicating much less shrinkage by adding nanofibers. (B) Shrinkage rate and density of NRPI-x aerogels. (C) Porosity of NRPI-x aerogels. The porosity of aerogels was calculated by $(1 - \rho_0/\rho) \times 100\%$, where ρ_0 is the apparent density, and ρ is the skeletal density, which is estimated from the density of polyimide (1.4 g cm^{-3}). (D) Schematic illustrating the good structural formability of NRPI-10, while NRPI-0 suffers from severe shrinkage.

process, resulting in lower shrinkage rate and higher structural integrity. Due to the reduction in shrinkage, there is a little decline in apparent density of NRPI aerogels with the increase of short polyimide nanofibers, which is reduced from 62.8 mg cm^{-3} (NRPI-0) to 54.4 mg cm^{-3} (NRPI-20) (Fig. 3B). With the increase of short polyimide nanofibers content, the porosity changes from 95.6% to 96.1%, which proves that the addition of short polyimide nanofibers has little influence on its porosity (Fig. 3C). This could be schematically illustrated in Fig. 3D. Short polyimide nanofibers serve as supports among pores and could inhibit the shrinkage during the freeze-drying and thermal imidization processes. In contrast, for NRPI-0, it will suffer from severe shrinkage as there exists no supporting structure in NRPI-0.

The mechanical properties of NRPI aerogels are investigated in Fig. 4. The stress-strain curves (Fig. 4A) indicate that NRPI aerogels could be compressed by 70% without serious collapse and could withstand a high strain even more than 90% without structure destruction (Fig. S3). The Young's modulus of NRPI aerogels is 1.8 ± 0.2 MPa, 2.2 ± 0.1 MPa, 3.7 ± 0.1 MPa and 1.3 ± 0.3 MPa for NRPI-0, NRPI-5, NRPI-10 and NRPI-20, respectively (Fig. 4B). The Young's modulus of NRPI aerogels generally increases concomitantly as the content of short polyimide nanofiber increase. The NRPI-10 aerogel exhibits the optimized

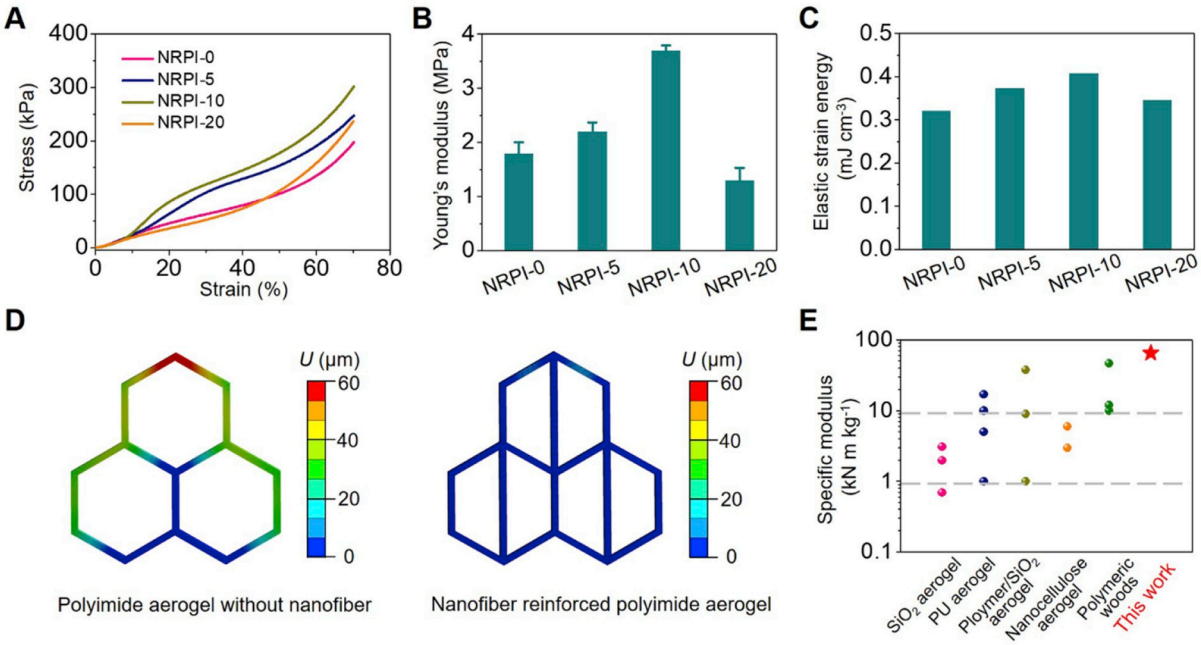

Fig. 4. Mechanical performance of NRPI aerogels. (A) Stress-strain curves, (B) Young's modulus, and (C) elastic strain energy of NRPI-x aerogels. (D) Finite element method (FEM) simulations of honeycomb structures with/without nanofiber reinforcement. The honeycomb structures are colored by the total displacement of element nodes. (E) Comparison of specific modulus of NRPI-10 with several common aerogel-like materials, including SiO_2 aerogels, PU aerogels, polymer/SiO_2 aerogels, nanocellulose aerogels, polymeric woods.

modulus, which is nearly twice that of NRPI-0 aerogel. The increasing modulus of NRPI aerogels with increasing nanofiber contents is due to the good interfacial interaction between nanofibers and matrix with homogeneity reinforcement, and nanofibers could help disperse stress along the pore wall and nanofibers. However, with further increasing of the content of short polyimide nanofibers, too much short polyimide nanofibers would aggregate as indicated by SEM image in Fig. S4, and the number of fiber ends and defects created by fiber ends increased [30], leading to the decreasing of Young's modulus for NRPI-20. Furthermore, the mechanical performance of NRPI aerogels with different lengths (0.2 mm, 0.3 mm, 0.4 mm) of short polyimide nanofibers is also investigated (Fig. S5). From strain-stress curves, it is observed that NRPI aerogel reinforced by short polyimide nanofibers with length of 0.3 mm shows better mechanical performance. The strength and modulus of short-fiber-reinforced composites normally increase with the increase of fiber length due to its higher aspect ratio (l/d). However, long fibers tend to bend or curl during molding, which causes reduction in the effective length of the fiber below the optimum length, leading to the deteriorated mechanical performance [31]. Therefore, short polyimide nanofibers with an optimum length of 0.3 mm are used in this study. The relative modulus and relative density of NRPI aerogels are shown in Fig. S6. Compared with neat polyimide aerogel, nanofiber reinforced polyimide aerogels show higher relative modulus with relative density changed a little, indicating that nanofibers can improve Young's modulus of aerogels without increasing the density. Elastic strain energy, which is defined as the ability of materials absorbing elastic deformation, is an important parameter to prove its toughness. As shown in Fig. 4C, from NRPI-0 to NRPI-10, the elastic strain energy increased from 0.32 mJ cm^{-3} to 0.40 mJ cm^{-3}, indicating that the addition of short polyimide nanofibers improved the toughness of aerogels. However, when the content of short polyimide nanofibers increases to 20%, elastic strain energy of NRPI aerogels will decrease, which might be due to that too much short polyimide nanofibers would aggregate as indicated by SEM image in Fig. S4. Furthermore, the NRPI aerogels exhibit an elastic performance at a low strain (25%) for 100 cycles without structure collapse as shown in Fig. S7. Finite element method (FEM) simulations were further conducted to explain the deformation mechanism of aerogels, where hexagonal hollow columns (Figs. S8 and S9) are used as an ideal model to help understand the underlying deformation and damage mechanisms of polyimide aerogels with/without nanofibers. As shown in Fig. 4D, for the porous honeycomb structure, the main failure is caused by the bending-dominated buckling of thin walls. For neat polyimide aerogels, the thin walls at the top would suffer from large stress under compression, leading to bending and warping of thin walls, resulting in low Young's modulus and strength of the aerogel. As for the nanofiber reinforced polyimide aerogel, the nanofibers would interconnect with the thin walls and help with stress transfer between thin walls. During the compression, this mode shows less stress concentration and stress would disperse along those supporting nanofibers (Fig. 4D). Thus, the NRPI aerogels show enhanced Young's modulus, attributing to the reinforcement of short nanofibers. As shown in Fig. 4E, the specific compression modulus (normalized by apparent density) of NRPI-10 aerogel is 65.7 kN m kg^{-1}, which outperforms the previously-reported aerogels including SiO_2 aerogel [32], PU aerogel [33,34], polymer/SiO_2 aerogel [35–39], nanocellulose aerogel [40] and polymeric woods [41].

Due to the high porosity and low density, aerogels show excellent thermal insulating performance. As shown in Fig. 5A, NRPI-0, without addition of short polyimide nanofibers, manifests a low thermal conductivity (41.2 ± 1.4 mW m^{-1} K^{-1}) similar to that of commercial insulating PS foams (35–43 mW m^{-1} K^{-1}) and PU foam (42–51 mW m^{-1} K^{-1}). Notably, the thermal conductivity for NRPI-5, NRPI-10 and NRPI-20 is 40.4 ± 2.8, 40.9 ± 1.2, and 38.8 ± 2.7 mW m^{-1} K^{-1}, respectively. The addition of short polyimide nanofibers into polyimide aerogels has little influence on thermal conductivity due to the similar pore structure and density of those aerogels. The low thermal conductivity of NRPI aerogels could be explained as follows. The measured total thermal conductivity of aerogels usually contains 4 components: radiative heat transfer coefficient (λ_r), convective heat transfer coefficient (λ_c), solid thermal conductivity (λ_s), and gas thermal conductivity (λ_g):

$$\lambda_{total} = \lambda_r + \lambda_s + \lambda_c + \lambda_g \quad (1)$$

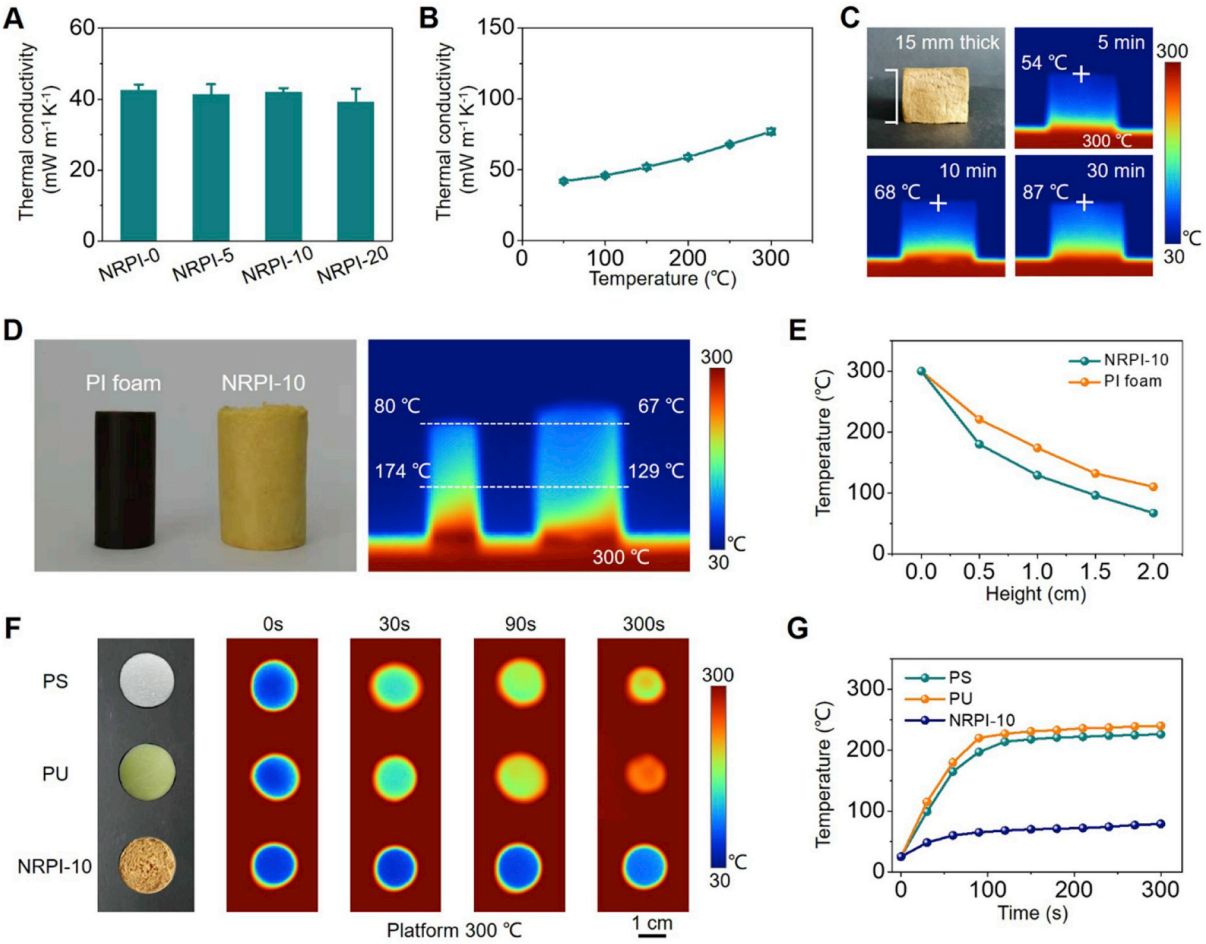

Fig. 5. Thermal insulating performance of NRPI aerogels. (A) Thermal conductivity of NRPI aerogels. (B) Thermal conductivity of NRPI-10 under different temperatures. (C) Infrared images of NRPI-10 on a hot stage of 300 °C for 5, 10 and 30 min. (D) Photograph and infrared images of commercial PI foams and NRPI-10 on a hot stage of 300 °C. (E) Temperature versus height of commercial PI foam and NRPI-10 obtained from infrared images. (F) The photograph and infrared images (taking from the top) of PU, PS and NRPI-10 on a hot stage of 300 °C with different times. (G) Surface temperature versus time of PS, PU and NRPI-10 obtained from infrared images.

For aerogels, the main heat transfer is contributed by heat conduction of solid and gas. The solid thermal conductivity (λ_s) is as follows:

$$\lambda_s = \lambda_{solid} * \frac{\rho \nu}{\rho_s \nu_s} \quad (2)$$

where λ_{solid} is the solid thermal conductivity of the basic materials, ρ is the apparent density, ρ_s is the skeletal density, ν is the velocity of phonon, and ν_s is the velocity of the phonon in the solid skeleton [42, 43]. Because of low density and solid fraction, NRPI aerogels exhibit a lower solid thermal conductivity (λ_s) compared with commercial thermal insulating materials. The interconnected 3D networks also reduce the solid thermal conductivity by creating more tortuous paths for polymer molecule to transport heat, leading to diffusive thermal transport. Intertwined 3D network of NRPI aerogels will prolong the motion path of air molecules, which will help to reduce gas thermal conductivity (λ_g) in NRPI aerogels. Furthermore, the high surface-to-volume ratio of nanofibers provides many solid-air interfaces, which improves reflectance of thermal fluent by creating a "multiple reflective effect". All the above factors make NRPI aerogels own low thermal conductivity. As shown in Fig. S10, the NRPI aerogels show similar thermal conductivity in different directions, indicating the isotropic feature of NRPI aerogels. More importantly, polyimide owns excellent thermal stability and its decomposition temperature is up to 400 °C as shown by thermogravimetric analysis in Fig. S11. Therefore, the NRPI aerogels show superior thermal insulating property at increased temperatures from 100 to 300 °C (Fig. 5B). The thermal conductivity of NRPI-10 shows a little increase with the increase of temperature, exhibiting a low thermal conductivity of 77.0 ± 2.1 mW m^{-1} K^{-1} at 300 °C. As a demonstration, the temperature change of NRPI-10 (15 mm thick) heated on a 300 °C stage for 30 min is shown in Fig. 5C. After heating for 30 min, the surface temperature of the sample is 87 °C, about 1/6 of the stage temperature, indicating its stability of thermal insulation for a long time. Then, we compared thermal insulating performance of NRPI-10 with commercial polyimide foam. Both NRPI-10 and commercial polyimide foam are placed on a hot stage with 300 °C. The surface temperature of NRPI-10 (20 mm thick) renders a much lower temperature (67 °C) compared with that (80 °C) of commercial polyimide foam (Fig. 5D). As shown in Fig. 5E, with decreased thickness, the NRPI-10 composite aerogel manifests a better thermal insulating property than the polyimide foam.

The thermal insulating performance of NRPI-10 aerogel is further compared with other common thermal insulating materials. PS foam, PU foam, and NRPI-10 aerogel with thickness of 1 cm are placed on the same hot stage (300 °C). The surface temperature of these samples is monitored by an infrared camera (Fig. 5F). Compared with PS foam and PU foam, NRPI-10 aerogel shows much lower surface temperature as time goes on, indicating its better thermal insulating performance. In the first 30 s, the surface temperatures of PS foam and PU foam exhibit a dramatic change, and start to degrade. However, the surface temperature of NRPI-10 aerogel is always the lowest with a little change. When at 300 s, PS foam and PU foam are degraded and lost thermal insulating

performance. However, the NRPI-10 aerogel remains original shape and still owns excellent thermal insulating performance. The surface temperature of NRPI-10 aerogel is stable at 67 °C after thermal equilibrium, which is significantly lower compared with that (above 200 °C) of PS foam and PU foam (Fig. 5G). Therefore, the excellent thermal insulating performance in wide temperature range makes NRPI aerogels as advanced thermal insulators.

4. Conclusions

In summary, NRPI aerogels have been prepared by using short electrospun polyimide nanofibers as reinforcing phase. The addition of short polyimide nanofibers makes NRPI aerogels exhibit low shrinkage (~25%), high porosity (>96%) and excellent structural stability. Due to the homogeneity reinforcement, short polyimide nanofibers could improve strength and toughness of polyimide aerogels by dispersing stress along the pore wall and nanofibers. The NRPI-10 with a low density exhibits good mechanical performance with compression modulus of 3.7 MPa, which is among the high level compared with polyimide aerogels by freeze-drying. Furthermore, due to the high porosity and intertwined 3D network, NRPI aerogels show good thermal insulating performance over a wide range of temperatures. The good mechanical property and low thermal conductivity make NRPI aerogels could find many potential applications such as in buildings, sport equipment and spacecrafts.

Author statement

Xingyu Zhao: Methodology, Investigation, Writing-Original draft preparation; **Fan Yang**: Data curation, Validation; **Zicheng Wang**: Investigation, Formal analysis; **Piming Ma**: Validation, Formal analysis, Data curation; **Weifu Dong**: Supervision; **Haoqing Hou**: Conceptualization, Methodology; **Wei Fan**: Conceptualization, Writing- Reviewing and Editing; **Tianxi Liu**: Supervision, Writing- Reviewing and Editing.

Declaration of competing interest

The authors declare that they have no known competing financial interests or personal relationships that could have appeared to influence the work reported in this paper.

Acknowledgements

The authors are grateful for the financial support from the National Natural Science Foundation of China (21674019, 21704014), the Fundamental Research Funds for the Central Universities (2232017D-06, 2232019A3-03), Shanghai Sailing Program (17YF1400200), Shanghai Municipal Education Commission (17CG33), and Ministry of Education of the People's Republic of China (6141A0202202). We greatly thank Jiangxi Advanced Nanofiber S&T Co., Ltd. for providing short polyimide nanofibers and Dr. Yiyu Feng from Tianjin University for the help with finite element method simulations.

Appendix A. Supplementary data

Supplementary data to this article can be found online at https://doi.org/10.1016/j.compositesb.2019.107624.

References

[1] Chu S, Majumdar A. Opportunities and challenges for a sustainable energy future. Nature 2012;488:294–303.
[2] Xu X, Zhang Q, Hao M, Hu Y, Lin Z, Peng L, et al. Double-negative-index ceramic aerogels for thermal superinsulation. Science 2019;363:723–7.
[3] Zhao S, Malfait WJ, Guerrero-Alburquerque N, Koebel MM, Nyström G. Biopolymer aerogels and foams: chemistry, properties, and applications. Angew Chem Int Ed 2018;5726:7580–608.
[4] Zhang L, Deng H, Fu Q. Recent progress on thermal conductive and electrical insulating polymer composites. Compos Commun 2018;8:74–82.
[5] Guo Y, Li K, Hou C, Li Y, Zhang Q, Wang H. Fluoroalkylsilane-modified textile-based personal energy management device for multifunctional wearable applications. ACS Appl Mater Interfaces 2016;87:4676–83.
[6] Chen S, Zheng Y, Zhang B, Feng Y, Zhu J, Xu J, et al. Cobalt, nitrogen-doped porous carbon nanosheet-assembled flowers from metal-coordinated covalent organic polymers for efficient oxygen reduction. ACS Appl Mater Interfaces 2019;111:1384–93.
[7] Li Y, Liu X, Nie X, Yang W, Wang Y, Yu R, et al. Multifunctional organic–inorganic hybrid aerogel for self-cleaning, heat-insulating, and highly efficient microwave absorbing material. Adv Funct Mater 2019;2910:1807624–32.
[8] Tian J, Shi Y, Fan W, Liu TX. Ditungsten carbide nanoparticles embedded in electrospun carbon nanofiber membranes as flexible and high-performance supercapacitor electrodes. Compos Commun 2019;12:21–5.
[9] Li L, Zhou J, Zhang C, Liu TX. Confined sulfidation strategy toward cobalt sulfide@nitrogen, sulfur co-doped carbon core-shell nanocomposites for lithium-ion battery anodes. Compos Commun 2019;15:162–7.
[10] Zuo L, Zhang Y, Zhang L, Miao YE, Fan W, Liu TX. Polymer/carbon-based hybrid aerogels: preparation, properties and applications. Materials 2015;810:6806–48.
[11] Nardecchia S, Carriazo D, Ferrer ML, Gutiérrez MC, del Monte F. Three dimensional macroporous architectures and aerogels built of carbon nanotubes and/or graphene: synthesis and applications. Chem Soc Rev 2013;422:794–830.
[12] Wicklein B, Kocjan A, Salazar-Alvarez G, Carosio F, Camino G, Antonietti M, et al. Thermally insulating and fire-retardant lightweight anisotropic foams based on nanocellulose and graphene oxide. Nat Nanotechnol 2014;10:277–83.
[13] Liao W, Wang G, Liu Z, Xu S, Wang Y-Z. Rheological premonitory of nanoclay morphology on the mechanical characteristics of composite aerogels. Compos B Eng 2019;173:106889–95.
[14] Abdelrahman EA, Hegazey RM. Exploitation of Egyptian insecticide cans in the fabrication of Si/Fe nanostructures and their chitosan polymer composites for the removal of Ni(II), Cu(II), and Zn(II) ions from aqueous solutions. Compos B Eng 2019;166:382–400.
[15] Ye X, Chen Z, Ai S, Hou B, Zhang J, Zhou Q, et al. Microstructure characterization and thermal performance of reticulated SiC skeleton reinforced silica aerogel composites. Compos B Eng 2019;177:107409–14.
[16] Jung IK, Gurav JL, Ha TJ, Choi SG, Baek S, Park HH. The properties of silica aerogels hybridized with SiO_2 nanoparticles by ambient pressure drying. Ceram Int 2012;38:105–8.
[17] Fan W, Zhang X, Zhang Y, Zhang Y, Liu T. Lightweight, strong, and super-thermal insulating polyimide composite aerogels under high temperature. Compos Sci Technol 2019;173:47–52.
[18] Fan W, Zuo L, Zhang Y, Chen Y, Liu T. Mechanically strong polyimide/carbon nanotube composite aerogels with controllable porous structure. Compos Sci Technol 2018;156:186–91.
[19] Si Y, Yu J, Tang X, Ge J, Ding B. Ultralight nanofibre-assembled cellular aerogels with superelasticity and multifunctionality. Nat Commun 2014;5:5802–11.
[20] Wang Y, Gao X, Fu Y, Wu X, Wang Q, Zhang W, et al. Enhanced microwave absorption performances of polyaniline/graphene aerogel by covalent bonding. Compos B Eng 2019;169:221–8.
[21] Jiang S, Uch B, Agarwal S, Greiner A. Ultralight, thermally insulating, compressible polyimide fiber assembled sponges. ACS Appl Mater Interfaces 2017;937:32308–15.
[22] Nam K-H, Jin J-U, Lee DH, Han H, Goh M, Yu J, et al. Towards solution-processable, thermally robust, transparent polyimide-chain-end tethered organosilicate nanohybrids. Compos B Eng 2019;163:290–6.
[23] Qian Z, Wang Z, Chen Y, Tong S, Ge M, Zhao N, et al. Superelastic and ultralight polyimide aerogels as thermal insulators and particulate air filters. J Mater Chem A 2018;63:828–32.
[24] Liao W, Zhao H-B, Liu Z, Xu S, Wang Y-Z. On controlling aerogel microstructure by freeze casting. Compos B Eng 2019;173:107036–50.
[25] Sung DH, Kang G-H, Kong K, Kim M, Park HW, Park Y-B. Characterization of thermoelectric properties of multifunctional multiscale composites and fiber-reinforced composites for thermal energy harvesting. Compos B Eng 2016;92:202–9.
[26] Qin Y, Peng Q, Ding Y, Lin Z, Wang C, Li Y, et al. Lightweight, superelastic, and mechanically flexible graphene/polyimide nanocomposite foam for strain sensor application. ACS Nano 2015;99:8933–41.
[27] Liu J, Zhang H-B, Xie X, Yang R, Liu Z, Liu Y, et al. Multifunctional, superelastic, and lightweight mXene/polyimide aerogels. Small 2018;1445:1802479–88.
[28] Wang JM, Liu D, Li QX, Chen C, Chen ZQ, Song PA, et al. Lightweight, superelastic yet thermoconductive boron nitride nanocomposite aerogel for thermal energy regulation. ACS Nano 2019;13:7860–70.
[29] Wu W, Wang K, Zhan M-S. Preparation and performance of polyimide-reinforced clay aerogel composites. Ind Eng Chem Res 2012;5139:12821–6.
[30] Sreenivasan VS, Ravindran D, Manikandan V, Narayanasamy R. Mechanical properties of randomly oriented short Sansevieria cylindrica fibre/polyester composites. Mater Des 2011;32:2444–55.
[31] Joseph K, Thomas S, Pavithran C, Brahmakumar M. Tensile properties of short sisal fiber-reinforced polyethylene composites. J Appl Polym Sci 1993;47:1731–9.
[32] Wong JCH, Kaymak H, Brunner S, Koebel MM. Mechanical properties of monolithic silica aerogels made from polyethoxydisiloxanes. Microporous Mesoporous Mater 2014;183:23–9.
[33] Diascorn N, Calas S, Sallée H, Achard P, Rigacci A. Polyurethane aerogels synthesis for thermal insulation-textural, thermal and mechanical properties. J Supercrit Fluids 2015;106:76–84.

[34] Chidambareswarapattar C, McCarver PM, Luo H, Lu H, Sotiriou-Leventis C, Leventis N. Fractal multiscale nanoporous polyurethanes: flexible to extremely rigid aerogels from multifunctional small molecules. Chem Mater 2013;2515:3205–24.
[35] Zhao S, Zhang Z, Sèbe G, Wu R, Rivera Virtudazo RV, Tingaut P, et al. Multiscale Assembly of superinsulating silica aerogels within silylated nanocellulosic scaffolds: improved mechanical properties promoted by nanoscale chemical compatibilization. Adv Funct Mater 2015;2515:2326–34.
[36] Zhao S, Malfait WJ, Demilecamps A, Zhang Y, Brunner S, Huber L, et al. Strong, thermally superinsulating biopolymer–silica aerogel hybrids by cogelation of silicic acid with pectin. Angew Chem Int Ed 2015;5448:14282–6.
[37] Katti A, Shimpi N, Roy S, Lu H, Fabrizio EF, Dass A, et al. Chemical, physical, and mechanical characterization of isocyanate cross-linked amine-modified silica aerogels. Chem Mater 2006;182:285–96.
[38] Meador MAB, Capadona LA, McCorkle L, Papadopoulos DS, Leventis N. Structure−property relationships in porous 3D nanostructures as a function of preparation conditions: isocyanate cross-linked silica aerogels. Chem Mater 2007;199:2247–60.
[39] Churu G, Zupančič B, Mohite D, Wisner C, Luo H, Emri I, et al. Synthesis and mechanical characterization of mechanically strong, polyurea-crosslinked, ordered mesoporous silica aerogels. J Sol Gel Sci Technol 2015;751:98–123.
[40] Kobayashi Y, Saito T, Isogai A. Aerogels with 3D ordered nanofiber skeletons of liquid-crystalline nanocellulose derivatives as tough and transparent insulators. Angew Chem Int Ed 2014;5339:10394–7.
[41] Yu Z-L, Yang N, Zhou L-C, Ma Z-Y, Zhu Y-B, Lu Y-Y, et al. Bioinspired polymeric woods. Sci Adv 2018;48:7223–32.
[42] Zhang F, Feng YY, Qin MM, Gao L, Li ZY, Zhao FL, et al. Stress controllability in thermal and electrical conductivity of 3D elastic graphene-crosslinked carbon nanotube sponge/polyimide nanocomposite. Adv Funct Mater 2019;29. 1901383.
[43] Qin MM, Xu YX, Cao R, Feng W, Chen L. Efficiently controlling the 3D thermal conductivity of a polymer nanocomposite via a hyperelastic double-continuous network of graphene and sponge. Adv Funct Mater 2018;28. 1805053.